Aspects of diffusion in the stadium billiard

Črt Lozej and Marko Robnik

CAMTP - Center for Applied Mathematics and Theoretical Physics, University of Maribor, Mladinska 3,
SI-2000 Maribor, Slovenia, European Union

We perform a detailed numerical study of diffusion in the ε stadium of Bunimovich, and propose an empirical model of the local and global diffusion for various values of ε with the following conclusions: (i) the diffusion is normal for all values of ε ($\leqslant 0.3$) and all initial conditions, (ii) the diffusion constant is a parabolic function of the momentum (i.e., we have inhomogeneous diffusion), (iii) the model describes the diffusion very well including the boundary effects, (iv) the approach to the asymptotic equilibrium steady state is exponential, (v) the so-called random model (Robnik *et al.*, 1997) is confirmed to apply very well, (vi) the diffusion constant extracted from the distribution function in momentum space and the one derived from the second moment agree very well. The classical transport time, an important parameter in quantum chaos, is thus determined.

I. INTRODUCTION

Billiard systems are very important model systems in classical and quantum chaos. One of the most studied billiards is the stadium billiard introduced by Bunimovich [1] in 1979, where it was proven to be rigorously ergodic and mixing. It is also a K system, as its maximal Lyapunov exponent is positive. In Fig. 1 we show and define the geometry and our notation of the stadium.

The radius of the two half circles is unity, while the length of the straight line is ε. By α we denote the angle of incidence, which is equal to the angle of reflection at the collision point. The phase space is defined by the Poincaré-Birkhoff coordinates (s,p), where s is the arclength parameter defined counterclockwise from $s = 0$ to $\mathcal{L} = 2\pi + 2\varepsilon$ ($\mathcal{L}$ is the length of the boundary), and the canonically conjugate momentum is $p = \sin\alpha$. As $s = 0$ and $s = \mathcal{L}$ are identified, we have a phase cylinder with the borders $p = \pm 1$. We assume that the billiard particle has unit speed. The discrete bounce map of the billiard Φ, connecting two successive collisions, $\Phi : (s,p) \to (s',p')$, is area preserving (see, e.g., [2]). For the circle billiard $\varepsilon = 0$ the momentum p, which is also the angular momentum, is a conserved quantity, while for small $\varepsilon > 0$ we observe slow chaotic diffusion in the momentum space p. The maximal Lyapunov exponent is positive for all values of $\varepsilon > 0$. A systematic study of the Lyapunov exponents in some representative chaotic billiards, including the stadium billiard, was published by Benettin [3], who has shown by numerical calculations that for small ε the Lyapunov exponent goes as $\propto \sqrt{\varepsilon}$. The diffusion regime of slow spreading of an ensemble of initial conditions in the momentum space has been observed in Ref. [4] and confirmed for $\varepsilon \leqslant 0.3$ in the present work. For larger $\varepsilon > 0.3$ the diffusion regime is hardly observable, as the orbit of any initial conditions quickly spreads over the entire phase space, already after a few ten collisions.

The characteristic time scale on which transport phenomena occur in classical dynamical systems is termed the "classical transport time" t_T. This is the typical time that an ensemble of particles needs to explore the available phase space. In classical chaotic billiards the characteristic diffusion time in momentum space is the relevant estimate for t_T. The present work was motivated by the study of chaotic billiards in the context of quantum chaos [5,6], in order to obtain good estimates of the characteristic times t_T which must be related or compared to the Heisenberg time t_H for the purpose of assessing the degree of quantum localization of chaotic eigenstates. The Heisenberg time is an important time scale in any quantum system with a discrete energy spectrum, defined as $t_H = (2\pi\hbar)/\Delta E$, where ΔE is the mean energy level spacing, i.e., the mean density of states is $\rho(E) = 1/\Delta E$. If t_H/t_T is smaller than 1, we observe localization, while for values larger than 1 we see extended eigenstates and the "principle of uniform semiclassical condensation" (PUSC) of Wigner functions applies. (See Refs. [7,8] and references therein.) Therefore a detailed investigation of the diffusion in the stadium billiard is necessary if the localization of the Wigner functions or Poincaré-Husimi functions should be well understood. This analysis is precisely along the lines of our recent works [8–10] for mixed type chaotic billiards, where the regular and (localized) chaotic eigenstates have been separated and the localization measure of the chaotic eigenstates has been introduced and studied. It was shown that the spectral statistics is uniquely determined by the degree of localization, which in turn is expected to be a unique function of the parameter t_H/t_T. This kind of analysis has been performed also for the quantum kicked rotator [11–14] by Chirikov, Casati, Izrailev, Shepelyansky, Guarneri, and further developed by many others. It was mainly Izrailev who has studied the relation between the spectral fluctuation properties of the quasienergies (eigenphases) of the quantum kicked rotator and the localization properties [14–16]. This picture has been recently extended in [17–20] and is typical for chaotic time-periodic (Floquet) systems. A similar analysis in the case of the stadium as a time independent system is in progress [21].

The study of diffusion in the stadium goes back to the early works of Casati and co-workers [4,22]. An excellent review
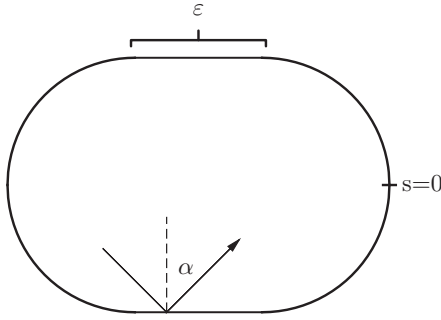
FIG. 1. The geometry and notation of the stadium billiard of Bunimovich.

of classical and quantum chaotic billiards was published by Prosen [23] with special interest in the quantum localization. Some of the analytic results about the diffusion constant have been obtained by the study of an approximate map [4], or of more general periodic Hamiltonian maps [24], along with the special case of the sawtooth map [25]. However, quite often not only the pointwise orbits but even the statistical properties of conservative dynamical systems exhibit extremely sensitive dependence on the control parameters and on initial conditions, as exemplified, e.g., in the standard map by Meiss [26]. The aforementioned studies used approximations of the stadium dynamics in order to obtain analytical results. Here we want to perform exact analysis of diffusion in the stadium billiard, which unavoidably must rest upon the numerical calculations of the exact stadium dynamics. Fortunately, the simple geometry of the stadium enables us to calculate the dynamics using analytical formulas subject only to round-off errors.

Thus far the study of momentum diffusion in the stadium billiard was, to the best of our knowledge, limited to the regime where ensembles are still narrow and far from the border of the phase space at $p = \pm 1$. The momentum diffusion there is normal and homogeneous and no border effects can be observed. In this work we extend this to include the global aspects of diffusion taking into account the finite phase space and the specifics of the billiard dynamics. As the stadium billiard is an archetype of systems with slow ergodicity many of our findings should be applicable to other systems sharing this trait.

The structure of the paper is as follows. In Sec. II we show that the chaotic diffusion is normal, but inhomogeneous, in Sec. III we do a detailed analysis of the variance of the distribution function and explore its dependence on the shape parameter ε and the initial conditions, in Sec. IV we examine the coarse grained dynamics and compare our results for the stadium with some preliminary results on a mixed type billiard defined in [27], and in Sec. V we discuss the results and conclude.

II. DIFFUSION IN THE STADIUM BILLIARD AND THE MATHEMATICAL MODEL

The study of diffusion in the stadium billiard was initiated in [4], where it was shown that for small ε we indeed see normal diffusion in the momentum space for initial conditions $p = 0$ and uniformly distributed on s along the boundary. For sufficiently short times (number of bounces), so that the spreading is close to $p = 0$, the diffusion constant can be

considered as p independent. Consequently the effects of the boundaries at $p = \pm 1$ are not yet visible. Moreover, it has been found [22] that the diffusion constant is indeed a function of the angular momentum, which for small ε coincides with p. Therefore we have to deal with inhomogeneous normal diffusion.

Our goal is to elaborate on the details of this picture. We begin with the diffusion equation for the normalized probability density $\rho(p,t)$ in the p space

$$\frac{\partial \rho}{\partial t} = \frac{\partial}{\partial p}\left(D(p)\frac{\partial \rho}{\partial p}\right). \tag{1}$$

The time t here is the continuous time, related to the "discrete time" N, the number of collisions, by $t = N\bar{l}$, where $\bar{l}$ is the average distance between two collision points and the speed of the particle is unity. In agreement with [22] the diffusion constant is assumed in the form

$$D(p) = D_0(\varepsilon)(1 - p^2), \tag{2}$$

where $D_0(\varepsilon)$ is globally an unknown, to be determined, function of the shape parameter ε. Note that in Ref. [22] the dependence of $D_0(\varepsilon)$ on the angular momentum was studied, while here we consider the dependence on p. It is only known that for sufficiently small ε, smaller than a characteristic value $\varepsilon_c \approx 0.1$ determined in the present work, or sufficiently larger than ε_c, we have the power law $D_0 = \gamma \varepsilon^\beta$, where the exponent β is 5/2 or 2 correspondingly, while our γ is a numerical prefactor, $\gamma \approx 0.13$ and 0.029, respectively, also to be analyzed later on. In the transition region, $\varepsilon \approx \varepsilon_c \approx 0.1$, we have no theoretical predictions and also the numerical calculations are not known or well established so far.

As we see in Eq. (1), the diffusion constant D is defined in such a way that the probability current density j is proportional to D and the negative gradient of ρ, that is $j = -D\, \partial \rho/\partial p$. Thus, the diffusion equation (1) is just the continuity equation for the probability (or number of diffusing particles), as there are no sources or sinks. For $p \approx 0$ and at fixed ε we can regard D as locally constant $D \approx D_0$. However, for larger $|p|$ we must take into account the dependence of D on p. Due to the symmetry the lowest correcting term in power expansion in p is the quadratic one, with the proportionality coefficient ν. For larger $|p|$, close to 1, the diffusion constant should vanish, so that near the border of the phase space cylinder $p = \pm 1$ there is no diffusion at all. These arguments lead to the assumption (2), which will be *a posteriori* justified as correct in our detailed empirical model.

Let us first consider the case of locally constant D at p around p_0, without the boundary conditions, i.e., the free diffusion on the real line p. Assuming initial conditions in the form of a Dirac δ distribution $\rho(p, t = 0) = \delta(p - p_0)$ peaked at $p = p_0$, we recover the well known Green function

$$\rho(p,t) = \frac{1}{2\sqrt{\pi D t}} \exp\left(-\frac{(p - p_0)^2}{4Dt}\right) \tag{3}$$

according to which the variance Var(p) is equal to

$$\langle (p - p_0)^2 \rangle = \int_{-\infty}^{\infty} \rho(p,t)(p - p_0)^2 dp = 2Dt. \tag{4}$$

This model is a good description for small ε and short times t.

However, for times comparable with the transport time the boundary conditions must be taken into account. There we assume that the *currents* on the boundaries $p = \pm 1$ must be zero, i.e., $\partial \rho / \partial p = 0$, so that the total probability in the momentum space is conserved and equal to unity. This will ultimately lead to the asymptotic equilibrium distribution $\rho(p,t) = 1/2$, with the variance $\mathrm{Var}(p) = 1/3$. The solution of the diffusion equation with these boundary conditions reads [28]

$$\rho(p,t) = \tfrac{1}{2} + \sum_{m=1}^{\infty} A_m \cos\left(\frac{m\pi}{2}(p+1)\right)$$
$$\times \exp\left(-\frac{Dm^2\pi^2 t}{4}\right). \quad (5)$$

Thus, the approach to the equilibrium $\rho = 1/2$ is always exponential. We will refer to this as the "homogeneous normal diffusion" model.

In the case of a δ function initial condition $\rho(p,t = 0) = \delta(p - p_0)$, we find by a standard technique $A_m = \cos[\frac{m\pi}{2}(p_0 + 1)]$. In the special case $p_0 = 0$ we have

$$\rho(p,t) = \frac{1}{2} \sum_{-\infty}^{\infty} \cos(m\pi p) \exp(-m^2\pi^2 Dt), \quad (6)$$

with the variance

$$\mathrm{Var}(p) = \langle p^2 \rangle = \frac{1}{3} + 4 \sum_{m=1}^{\infty} \frac{(-1)^m}{m^2\pi^2} \exp(-m^2\pi^2 Dt), \quad (7)$$

which approaches exponentially the equilibrium value $\mathrm{Var}(p) = 1/3$ at large time t,

$$\mathrm{Var}(p) \approx \frac{1}{3} - \frac{4}{\pi^2} \exp(-\pi^2 Dt), \quad (8)$$

where the higher exponential terms $m > 1$ have been neglected.

Next we want to understand the behavior of the diffusion when the full general expression for the p-dependent diffusion constant D, defined in (2), is taken into account. We find the solution (see also [29]) in terms of the Legendre polynomials $P_l(p)$ as follows:

$$\rho(p,t) = \sum_{l=0}^{\infty} A_l P_l(p) \exp[-l(l+1)D_0 t], \quad (9)$$

where the expansion coefficients A_l expressed by the initial conditions at time $t = t_0$ are

$$A_l = \frac{2l+1}{2} \int_{-1}^{1} P_l(p)\rho(p,t = t_0)dp. \quad (10)$$

It can be readily verified that the solution (9) satisfies the diffusion equation (1) with $D = D_0(1 - p^2)$ as in (2). It also satisfies the boundary conditions of vanishing currents at $p = \pm 1$, since $D = 0$ there. Because the set of all Legendre polynomials is a complete basis set of functions on the interval $-1 \leqslant p \leqslant 1$, an arbitrary initial condition may be satisfied. Therefore (9) is the general solution. From (9) we also see that $\rho(p,t)$ approaches its limiting value A_0 exponentially, and moreover, in (10) that for any normalized initial condition we

have $A_0 = 1/2$. We will refer to this as the "inhomogeneous normal diffusion" model.

For a general diffusion constant $D(p)$ that is an even function of p, which in our case is due to the physical p-inversion symmetry in the phase space, we can derive a general equation for the moments and variance of p. Starting from Eq. (1) and using the boundary conditions we first show that the total probability is conserved. Second, for the centered initial condition $p_0 = 0$, that is $\rho(p,t = 0) = \delta(p)$, we find that the first moment vanishes $\langle p \rangle = 0$, and for the time derivative of the variance we obtain

$$\frac{d\langle p^2 \rangle}{dt} = -4\rho(1,t)D(1) + 2\int_{-1}^{1} \rho(p)\frac{d[pD(p)]}{dp}dp. \quad (11)$$

In the special case $D = D_0(1 - \nu p^2)$ we get the differential equation

$$\frac{d\langle p^2 \rangle}{dt} = -4\rho(1,t)D(1) + 2D_0(1 - 3\nu\langle p^2 \rangle). \quad (12)$$

This is an interesting quite general result. In our system we have $\nu = 1$, therefore $D(1) = 0$, and we find for the variance the explicit result by integration

$$\langle p^2 \rangle = \tfrac{1}{3}[1 - \exp(-6D_0 t)]. \quad (13)$$

Thus, again, the approach to equilibrium value $\mathrm{Var}(p) = 1/3$ is exponential, with the important classical transport time $t_T = 1/(6D_0)$. If this equation is rewritten in terms of the discrete time N (the number of collisions), then $t = N\bar{l}$, and we find

$$\langle p^2 \rangle = \frac{1}{3}\left(1 - \exp\left(-\frac{N}{N_T}\right)\right), \quad (14)$$

where "the discrete classical transport time" N_T is now defined as

$$N_T = \frac{1}{6D_0\bar{l}}. \quad (15)$$

Here $\bar{l}$ is the average distance between two successive collision points. We also define the discrete diffusion constant as $D_{\mathrm{dis}} = D_0\bar{l}$. In the case of ergodic motion the mean free path $\bar{l}$ as a function of the billiard area $\mathcal{A}$ and the length $\mathcal{L}$ is known to be [30]

$$\bar{l} = \frac{\pi\mathcal{A}}{\mathcal{L}} = \frac{\pi(\pi + 2\varepsilon)}{2\pi + 2\varepsilon} \approx \frac{\pi}{2}. \quad (16)$$

Thus, by measuring D_{dis} we determine N_T, which plays an important role in quantum chaos when related to the Heisenberg time [9,10], $t_H/t_T = 2k/N_T = 2\sqrt{E}/N_T$, as discussed in the Introduction. Here $E = k^2$ is the energy of the billiard particle.

It is well known that the bouncing ball modes (the continuous family of period two periodic orbits), within $s \in (\pi/2, \pi/2 + \varepsilon)$ and $s \in (3\pi/2 + \varepsilon, 3\pi/2 + 2\varepsilon)$ and $p = 0$ present sticky objects in the classical phase space, as illustrated in Fig. 2. If we choose initial conditions inside these bouncing ball areas, we find a centrally positioned δ peak which never decays. Moreover, even orbits close to these bouncing ball areas stay inside for very long times, because the transition times for exiting (and also entering) these regions are very large. Such correlations have been studied in Refs. [31,32].

Therefore in studying the diffusion in the momentum space emanating from $\rho(p,t = 0) = \delta(p - p_0)$ we have used the
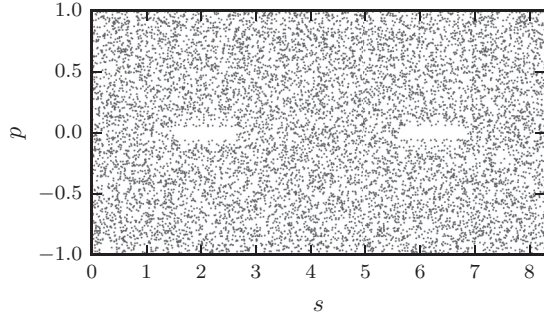
FIG. 2. The phase space of the stadium for $\varepsilon = 1$, with 10^4 bounces along an orbit emanating from ($s = \pi/4, p = 0$), showing the avoidance of the bouncing ball areas.

initial conditions $p_0 = 0$ and uniformly distributed over the s excluding the two intervals $s \in (\pi/2 - \varepsilon, \pi/2 + 2\varepsilon)$ and $s \in (3\pi/2, 3\pi/2 + 3\varepsilon)$, to exclude the slowly decaying peak in the distribution located at $p = 0$. The result for $\varepsilon = 0.1$ is shown in Fig. 3. As we see, the model of the inhomogeneous diffusion Eq. (9) is a significant improvement over the model of homogeneous diffusion Eq. (6) and works very
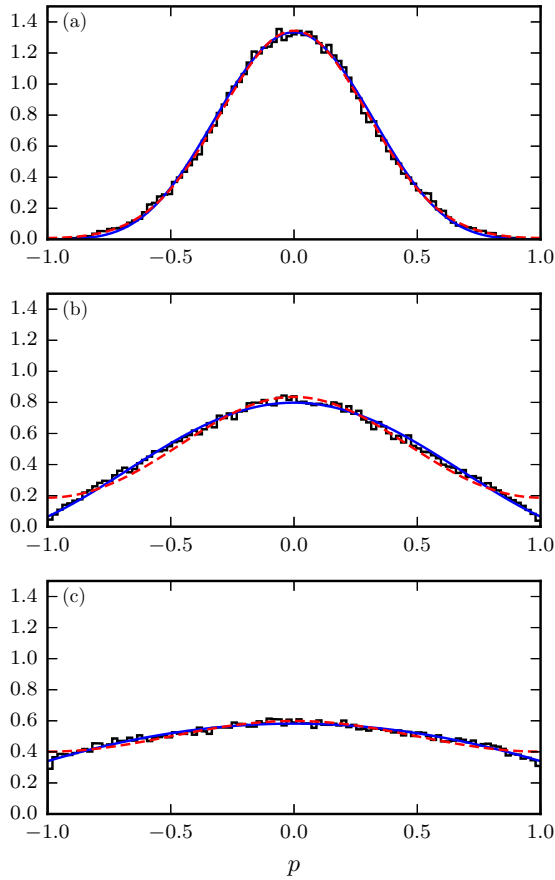

FIG. 3. The distribution function $\rho(p, N)$ after $N = 100$ collisions (a), $N = 300$ collisions (b), and $N = 700$ collisions (c). The 10^5 initial conditions at $p_0 = 0$ are as described in the text. $\varepsilon = 0.1$. The blue full line is the theoretical prediction for the inhomogeneous diffusion (9), the dashed red curve corresponds to the homogeneous diffusion (6).
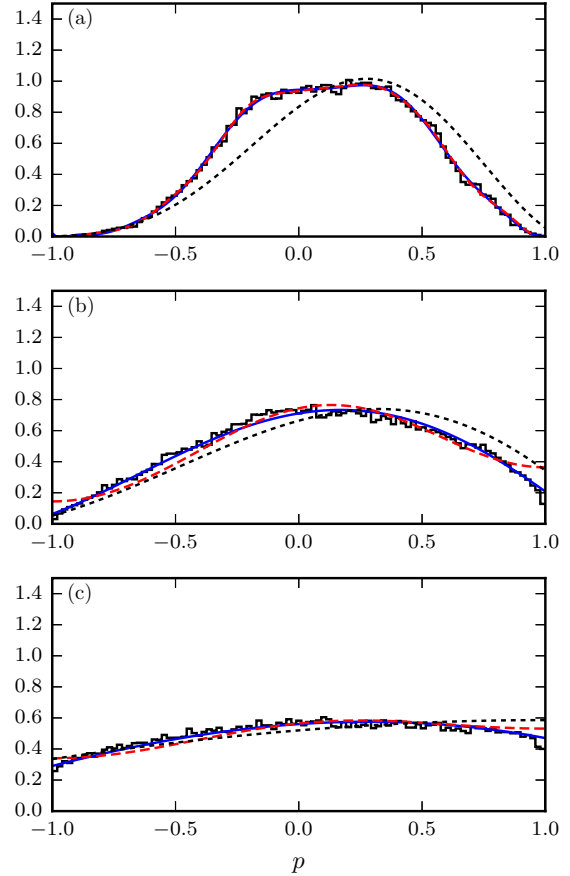

FIG. 4. The distribution function $\rho(p, N)$ after $N = 100$ collisions (a), $N = 300$ collisions (b), and $N = 700$ collisions (c). The 10^5 initial conditions at $p_0 = 0.25$ are uniformly distributed over $s \in [0, \mathcal{L})$, and are taken at $N = 100$ collisions. $\varepsilon = 0.1$. The blue full line is the theoretical prediction for the inhomogeneous diffusion (9), the long-dashed red curve corresponds to the homogeneous diffusion (6), while the short-dashed black line is the theoretical prediction of the inhomogeneous diffusion starting from the initial δ spike $\rho(p, t = 0) = \delta(p - p_0)$ rather than from the delayed histogram of (a).

well. The results are the same if we take the ensemble of initial conditions randomly and uniformly spread in a thin strip $p_0 \in [-0.01, 0.01]$.

Although we shall study the dependence of statistical properties on initial conditions in Sec. III, we should explore the time evolution of the diffusion in the momentum space for nonzero initial conditions $p_0 \neq 0$ already at this point, starting from $\rho(p, t = 0) = \delta(p - p_0)$, where now the 10^5 initial conditions are uniformly distributed over all $s \in [0, \mathcal{L})$. It turns out that there is some transient time period, where the diffusive regime is not yet well established, which we demonstrate for $\varepsilon = 0.1$ in Figs. 4–6 for $p_0 = 0.25$, 0.50, and 0.75, correspondingly. The black short-dashed curve corresponds to the theoretical prediction based on the inhomogeneous diffusion model (9) starting with the initial δ spike $\rho(p, t = 0) = \delta(p - p_0)$, and the initial conditions are uniform on all $s \in [0, \mathcal{L})$. The red long-dashed curve corresponds to the homogeneous diffusion model (6), the blue full line corresponds to the inhomogeneous diffusion model (9). In both latter cases
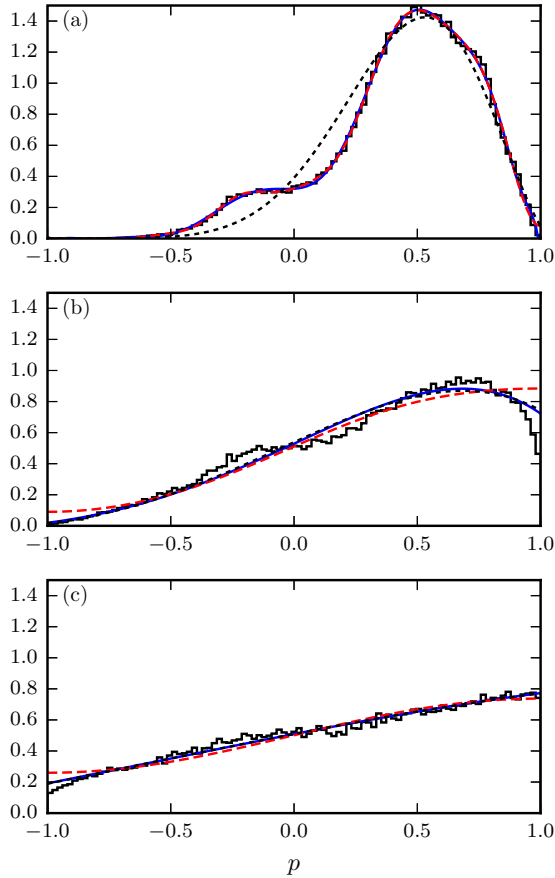
FIG. 5. As in Fig. 4 but with $p_0 = 0.50$.
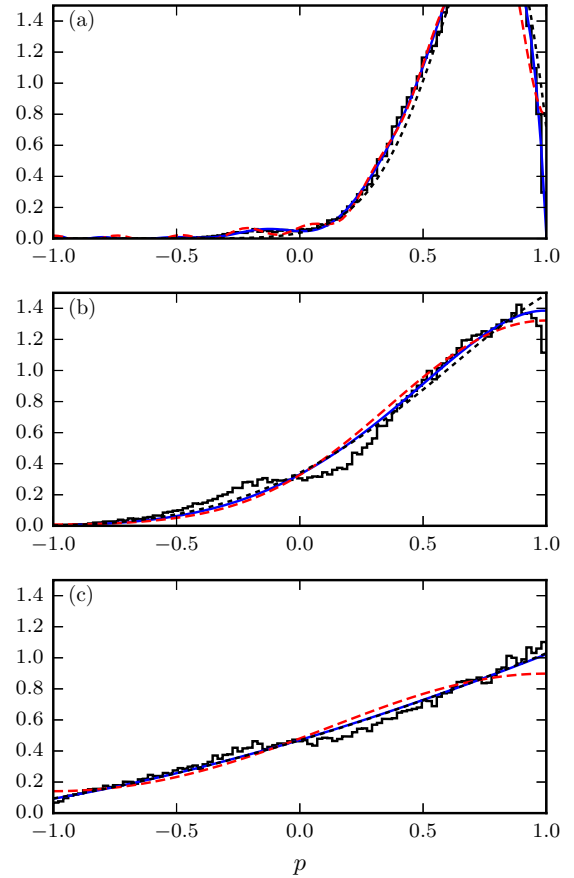
FIG. 6. As in Fig. 4 but with $p_0 = 0.75$.

the initial conditions were taken from the histogram at the time of 100 collisions, and the coefficients in Eqs. (5), (6), (9), and (10) were determined. The delay of 100 collisions has been chosen due to the initial transient behavior where the diffusion is not yet well defined. Nevertheless, the time evolution of the diffusion excellently obeys the inhomogeneous law (9) for longer times.

In these plots we observe qualitatively good agreement with the theory, except for some visible deviation of the numerical histogram from the theoretical prediction, around $p \approx 0$ in Figs. 5 and 6. We believe that these effects are related to sticky objects around the bouncing ball areas whose existence is demonstrated in the phase space plot of Fig. 2, and is thus a system-specific feature, which would disappear in a "uniformly ergodic" system. However, it must be admitted that chaotic billiards often have such continuous families of marginally stable orbits [33].

III. ANALYSIS OF THE VARIANCE OF THE DISTRIBUTION FUNCTION

In order to determine the value of the diffusion constant D_0 and its dependence on ε as defined in Eqs. (1) and (2) we can use either the evolution of the entire distribution function $\rho(p,t)$ or of its second moment, the variance. When this was done in special cases, agreement has been found. However, the second moment of the distribution function is much more

stable than the distribution function itself, so we have finally decided to use the variance of p to extract the value of D_0 from Eq. (13), where the δ spike initial condition at $p_0 = 0$ is assumed. This approach would be ideal, if our model of the inhomogeneous diffusion in Eqs. (1), (2), (9), and (10) were exact.

However, this is not the case due to the bouncing ball regions described in the previous section and the fact that the diffusive regime is not yet well established for short times. Moreover, even if the model were exact, Eq. (13) does not apply to initial conditions at nonzero p_0. The variance for the more general initial conditions $\rho(p,t=0) = \delta(p - p_0)$ is easily obtained by calculating the first two moments of the distribution (9). This is done by inserting the initial conditions into Eq. (10) and using the orthogonality relations of the Legendre polynomials. The average momentum is given by

$$\langle p \rangle = p_0 \exp(-2D_0 t), \tag{17}$$

and the variance by

$$\begin{aligned}
\mathrm{Var}(p) &= \langle p^2 \rangle - (\langle p \rangle)^2 \\
&= \tfrac{1}{3}[1 - \exp(-6D_0 t)] + p_0{}^2 \exp(-6D_0 t) \\
&\quad - p_0{}^2 \exp(-4D_0 t). \tag{18}
\end{aligned}$$

As we see there is no clear way to define the transport time since two exponential functions with different exponents are present.
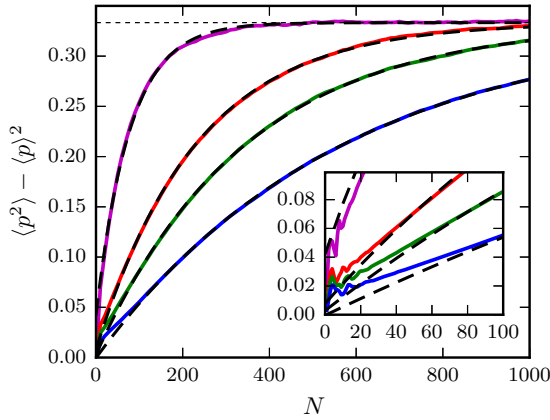
FIG. 7. The variance of p as a function of the number of collisions N for four different values of ε, starting at the initial condition $p_0 = 0$. From top to bottom we show the numerical results for $\varepsilon = 0.2$ (magenta), $\varepsilon = 0.12$ (red), $\varepsilon = 0.1$ (green), $\varepsilon = 0.08$ (blue) calculated with 10^5 initial conditions. The theoretical fitting curves according to Eq. (19) are shown with black dashed lines. The inset is a magnification of the first 100 bounces and shows the initial nondiffusive phase.

FIG. 8. The variance as a function of the number of collisions N for $\varepsilon = 0.1$, starting at four initial conditions $p_0 = 0, 0.25, 0.50, 0.75$. Each curve is shifted upwards by 0.1 in order to avoid the overlapping of curves. They all converge to $1/3$ when $N \to \infty$. The dotted black curve shows the theoretical prediction for the variance (18), while the dashed curve shows the empirical model (19).

Furthermore, as we saw earlier in Figs. 4–6 the diffusive regime is only well established after enough time has passed. We therefore chose to empirically generalize Eq. (14) by the introduction of a prefactor C as follows:

$$\text{Var}(p) = \frac{1}{3}\left[1 - C \exp\left(-\frac{N}{N_T}\right)\right]. \quad (19)$$

As we shall see the prefactor C effectively compensates the generalized initial conditions and allows us to estimate the transport time.

In Fig. 7 we show the evolution of the variance as a function of the number of collisions, for four different values of $\varepsilon = 0.08, 0.10, 0.12, 0.20$. The initial conditions are the same as in Fig. 3 of Sec. II. The agreement with the empirical model (19) [which in this case coincides with the theoretical prediction (14) if $C = 1$] is excellent. The inset shows the initial nondiffusive phase of the dynamics. The fitting procedure was as follows: first, N_T has been extracted from the best fitting of all data, and then the fitting was repeated by excluding the first 20% of collisions, but not less than 20 of them, up to maximum of 300 collisions, in order to be in the optimal interval for the determination of the two fitting parameters N_T and C and to exclude the nondiffusive phase.

Finally, we take a fixed value of $\varepsilon = 0.1$ and observe the variance as a function of discrete time N for various values of the initial condition $\delta(p - p_0)$, $p_0 = 0., 0.25, 0.50, 0.75$, and use the same fitting procedure. The initial conditions are the same as in Figs. 3–6, correspondingly. Again, the agreement with the empirical formula (19) is excellent, as is seen in Fig. 8. The variance is well described also by the theoretical prediction Eq. (18), particularly for larger values of p_0. From there we may extract the value of $D_{\text{dis}} = D_0 \bar{l}$. Note that for $p_0 = 0$ the two descriptions coincide. Alternatively we could also extract the values of D_{dis} from the average of the momenta using Eq. (17). This yields equivalent results for values of $p_0 > 0.35$, but for lower nonzero values, Eq. (17) fails to correctly describe the
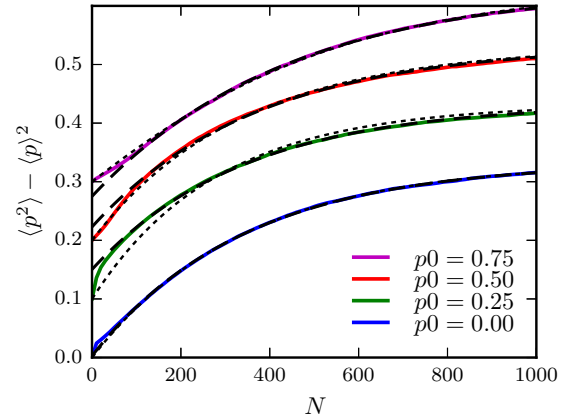
numerical time dependent averages. This is because the initial nondiffusive phase significantly changes the average of the distribution of momenta from the one predicted from the initial δ distribution (compare the histogram with the black dashed line in Fig. 4). This effect is diminished for $p_0 > 0.35$, probably because the peak of the distribution is further from the area of phase space near the marginally unstable bouncing ball orbits (see Figs. 5 and 6).

In Table I we present the list of values of N_T at $p_0 = 0$, as a function of ε, extracted by the described methodology. They are important in understanding the quantum localization of chaotic eigenstates as previously discussed.

In Fig. 9 we show the result for the diffusion constant in terms of the discrete time N, that is $D_{\text{dis}} = D_0 \bar{l}$, as a function of ε, as well as C as a function of ε, with the initial conditions $\rho(p, t = 0) = \delta(p - p_0)$ at $p_0 = 0$.

We clearly observe the confirmation of the two limiting power laws $D_{\text{dis}} \propto \varepsilon^{5/2}$ for small ε and $D_{\text{dis}} \propto \varepsilon^2$ for large ε. In the transition region $\varepsilon \approx \varepsilon_c \approx 0.1$ which is about half of a decade wide, the analytic description is unknown.

The dependence of D_{dis} in accordance with Eq. (18) on the parameter p_0 for the special case $\varepsilon = 0.1$ is shown in Fig. 10(a). The value of D_{dis} is minimal at $p_0 = 0$. This may be because the phase space contains sticky objects near the marginally unstable bouncing ball orbits. Here we must understand that at larger times, asymptotically, the initial conditions are forgotten, and we expect that D_{dis} tends to a constant value which is the case. The values of D_{dis} at $p_0 = 0.75$ exhibit the same power law dependencies on ε as those at $p_0 = 0$. N_T and C in accordance with Eq. (19) are shown in Figs. 10(b) and 10(c). The value of N_T increases for larger values of p_0. This is an effect of the local transport being slower in the vicinity of the border $p = \pm 1$ due to the parabolic diffusion law (2). The shortest estimate for the classical transport time, the one at $p_0 = 0$, is the one relevant for the study of localization of the eigenstates of the quantum billiard.

TABLE I. The discrete transport time N_T (number of collisions) as function of ε as defined in Eq. (19), with initial conditions at $p_0 = 0$, and therefore Eq. (14) also applies. The sizes of the ensembles were 10^5 for $\varepsilon < 0.02$, 2.5×10^5 for $0.02 \leqslant \varepsilon < 0.08$ and 10^6 for $\varepsilon > 0.08$.

	Transport times		
ε	N_T	ε	N_T
0.001	3×10^7	0.105	303
0.005	4.3×10^5	0.110	275
0.010	7.8×10^4	0.115	253
0.015	2.9×10^4	0.120	233
0.020	1.4×10^4	0.125	215
0.025	8410	0.130	299
0.030	5520	0.135	186
0.035	3750	0.140	172
0.040	2760	0.145	161
0.045	2110	0.150	150
0.050	1630	0.155	141
0.055	1340	0.160	131
0.060	1100	0.165	123
0.065	907	0.170	115
0.070	767	0.175	108
0.075	647	0.180	102
0.080	560	0.185	95
0.085	494	0.190	90
0.090	433	0.195	86
0.095	386	0.200	82
0.100	341		

FIG. 10. $D_{\text{dis}} = D_0 \bar{l}$ from (18), and N_T with C from (19) as functions of p_0 for $\varepsilon = 0.1$.
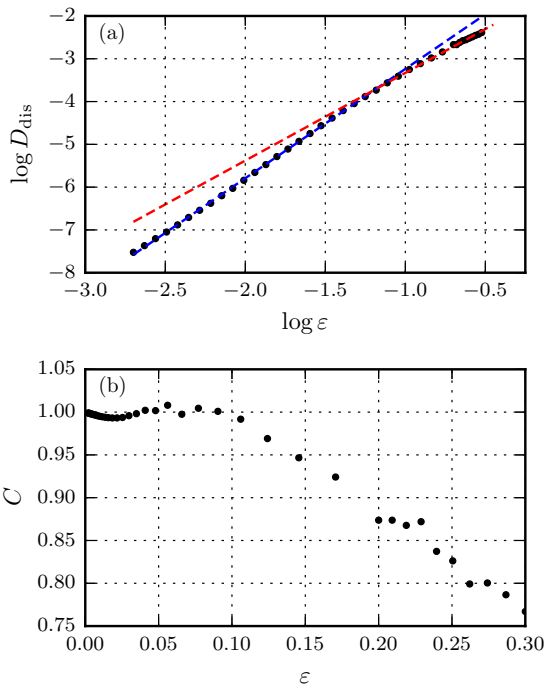

FIG. 9. $D_{\text{dis}} = D_0 \bar{l} = 1/(6N_T)$ and C as functions of ε, at $p_0 = 0$, using the Eq. (19). The log is decadic. Ideally, C should be unity according to Eqs. (13) and (14).
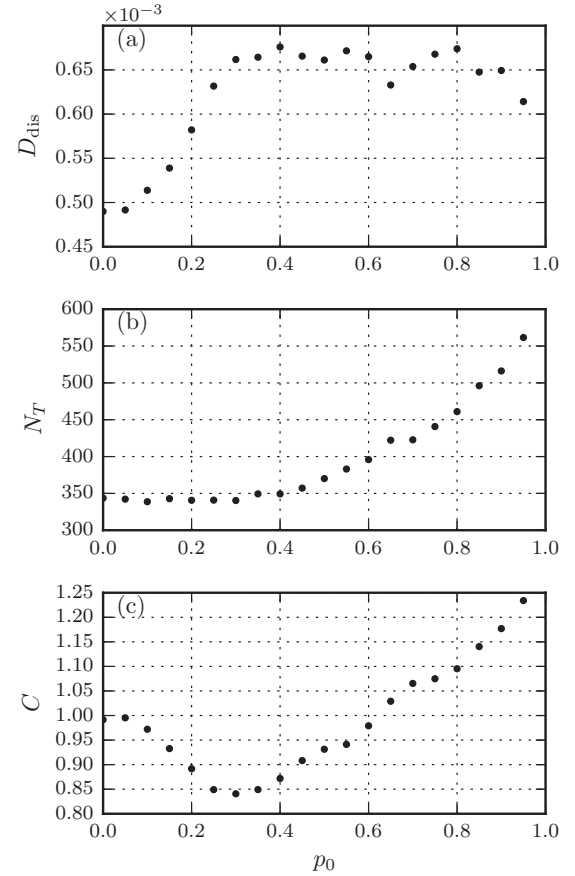
IV. COMPARISON OF CHAOTIC DIFFUSION IN A MIXED TYPE BILLIARD

In this section we study the coarse grained dynamics of the stadium billiard. We partition the phase space into a grid of cells and record the number of times each cell is visited by the orbit. It is interesting to briefly discuss the observed differences between ergodic systems like the stadium and the behavior in the chaotic components of mixed type systems. Examples are the billiard introduced in [27], the border of which is given by a conformal mapping of the unit circle in the complex plane $|z| = 1$,

$$z \rightarrow z + \lambda z^2, \qquad (20)$$

at various shape parameter values λ and the standard map [26]. In the case of $\lambda = 1/2$ the billiard was proven to be ergodic [34]. Because this billiard is strongly chaotic the classical transport time is of the order of a few ten bounces. An analysis of the diffusion along the lines of the previous sections is therefore not possible.

The first important observation is, that the so-called *random model* (Poissonian filling of the coarse grained network of cells in the phase space) introduced in [35], works very well in the stadium and also in other ergodic systems like $\lambda = 1/2$ billiard. In the process of filling, the cells are considered as filled (occupied) as soon as the orbit visits them. The approach to the asymptotic value 1 for the relative size of the filled
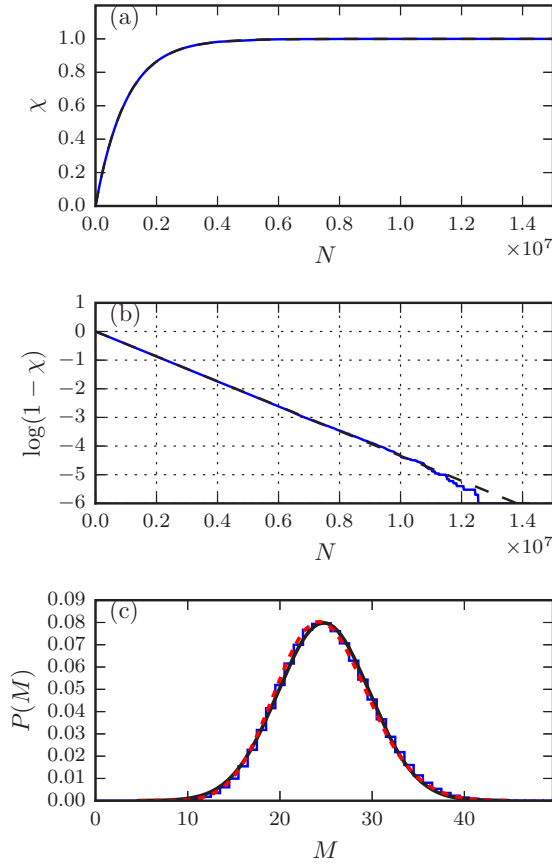
FIG. 11. The filling of the cells $\chi(N)$ for the stadium billiard $\varepsilon = 0.1$ in the lin-lin plot (a), the decadic log-lin plot (b) and the distribution of cells with the occupancy number M (c). The black dashed curve in (a) and (b) is the random model Eq. (21). There are 25×10^6 collisions and $N_c = 10^6$ cells, so that the mean occupancy number $\mu = \langle M \rangle = 25$. The chaotic orbit has the initial conditions ($s = \pi/4, p = 0$). The black full curve is the best fitting Gaussian, while the red dashed curve is the best fitting Poissonian distribution. The theoretical values μ and $\sigma^2 = \mu b = \mu(1 - a)$ and their numerical values agree very well.

chaotic component χ as a function of the discrete time (number of collisions) N is exponential,

$$\chi(N) = 1 - \exp\left(-\frac{N}{N_c}\right). \tag{21}$$

where N_c is the number of cells. This is demonstrated in Fig. 11 for the case $\varepsilon = 0.1$, where chaos, dependence on initial conditions due to the large Lyapunov exponent, is strong, and agreement with the random model is excellent, while for the case $\varepsilon = 0.01$ chaos is weak, and the agreement is not so good as seen in Fig. 12.

In both cases we show the lin-lin plot of (21) in (a), and also the log-lin plot in (b) for $1 - \chi$. In (c) we show the distribution of the occupancy number M of cells, which clearly is very close to a Gaussian. The size of the grid of cells is $L = 1000$, thus $N_c = L^2 = 10^6$.

The latter observation can be easily explained by the following theoretical argument within the Poissonian picture. We start an orbit in one of the N_c cells of the chaotic region and follow its evolution for a fixed number of collisions N. Let
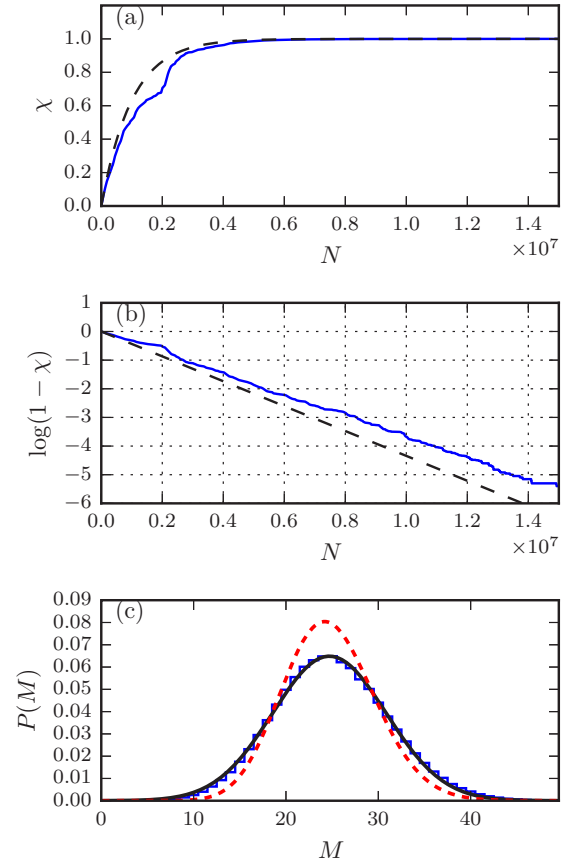

FIG. 12. As in Fig. 11 but $\varepsilon = 0.01$. Some deviations from the random model are seen, which are always negative due to the sticky objects in the phase space which delay the diffusion.

$a = 1/N_c$ be the uniform probability that at the given discrete time N one of the cells will be visited (by the orbit), while its complement $b = 1 - a$ is the probability that the cell will not be visited. As we assume absence of any correlations between the visits, the calculation of the distribution of the occupancy M of the cells is easy: The probability $P(M)$ to have a cell containing M visits is simply the binomial distribution

$$P_B(M) = \binom{N}{M} a^M b^{N-M}, \tag{22}$$

which has the exact values for the mean and variance

$$\mu = \langle M \rangle = Na, \quad \sigma^2 = \langle (M - \mu)^2 \rangle = Nab = \mu b. \tag{23}$$

For sufficiently large N this can be approximated by the Gaussian with the same μ and σ^2,

$$P_G(M) = \frac{1}{\sqrt{2\pi\sigma^2}} \exp\left(-\frac{(M - \mu)^2}{2\sigma^2}\right). \tag{24}$$

In the Poissonian limit $a \to 0$ and $N \to \infty$, but $\mu = aN = $ const, we find the Poissonian distribution

$$P_P(M) = \frac{\mu^M e^{-\mu}}{M!}. \tag{25}$$

We see that the mean value and the variance agree with the theoretical prediction $\mu = N/N_c = 25$ and $\sigma^2 = \mu b \approx \mu = 25$, so that the standard deviation $\sigma = 5$, in the case of
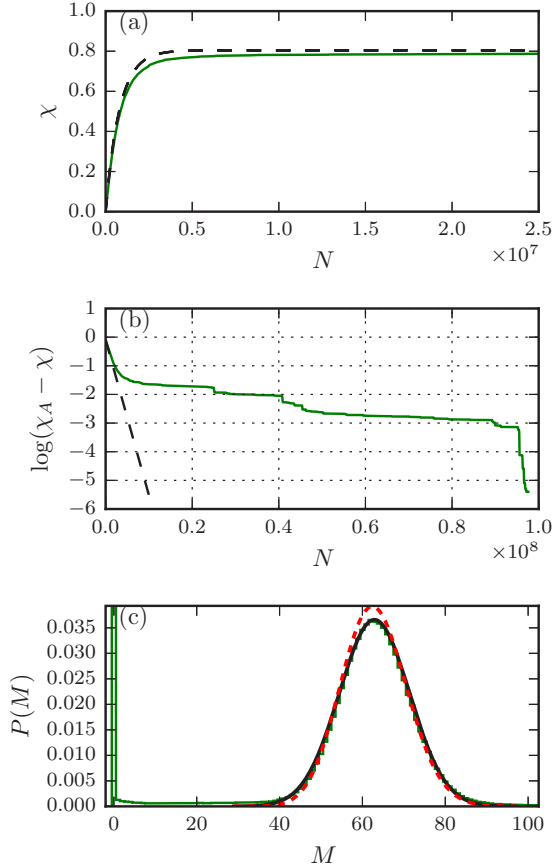
FIG. 13. As in Fig. 11 but for the mixed type billiard [27] with $\lambda = 0.15$, for an orbit with 10^8 collisions. The asymptotic value of χ is $\chi_A = 0.80$, as we see in (a). Large deviations from the random model are seen also in (b), which are always negative due to the sticky objects in the phase space which delay the diffusion. In (c) we see the distribution of cells at time $N = 5 \times 10^7$ according to the occupancy M, which now consists of the the Gaussian bulge corresponding to the cells of the largest chaotic region, and the δ peak at $M = 0$ corresponding to the regular and other smaller chaotic regions. The initial condition (using the standard Poincaré-Birkhoff coordinates) is $(s = 4.0, \; p = 0.75)$.

$\varepsilon = 0.1$. However, in the case $\varepsilon = 0.01$ we see a quantitative discrepancy with the random model prediction in Fig. 12(a), but nevertheless the approach to the asymptotic values is exponential with a slightly different coefficient (b). Due to the sticky objects the filling of the cells is slower. The variance of the distribution in (c) is 38, which is larger than the predicted value $\mu b = 25$, meaning that the relative fraction of more and of less richly occupied cells is larger than expected by the binomial distribution. Note that the Poisson distribution with the same μ (dashed red) significantly deviates from the histogram.

In the chaotic components of mixed type systems things are different. The random model does not work well, the approach to the equilibrium value is not exponential, but instead is perhaps a power law as reported by Meiss [26], or even something else as observed in our work [36]. Here we just show for comparison in Fig. 13 the time dependence of the relative fraction of occupied cells $\chi(N)$ for the billiard introduced in
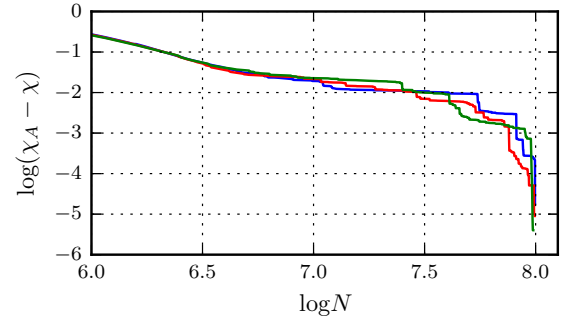

FIG. 14. As in Fig. 13(b) but now in decadic log-log plot to show that the approach to the asymptotic value χ_A is neither an exponential function nor a power law. The curves correspond to three different initial conditions, $(s, p) = (4.0, 0.75), (2.5, 0.75), (2.5, 0.15)$, in green, blue, and red correspondingly.

[27] with the shape parameter $\lambda = 0.15$ (a slightly deformed circle), in analogy with Figs. 11 and 12.

It is clear that the random model is not good, and the approach to the asymptotic value $\chi_A \approx 0.80$ is neither exponential nor a power law, but something different to be studied further [36], as one can see in the lin-lin plot (a) and in the log-lin plot in (b) of Fig. 13, and also in Fig. 14 for three different initial conditions. The selected initial conditions are well separated yet yield very similar results. We therefore expect an ensemble average would not change the overall shape of the curve.

One should note that the measured $\chi(N)$ is always below the prediction of the random model, which is due to the sticky objects in the phase space, that delay the diffusion process, and occasionally also cause some plateaus on the curve (due to temporary trapping). Also the cell occupancy numbers shown in (c) are different from the simple binomial distribution for the cells. Clearly, the empty cells at $M = 0$ represent the regular part of the phase space, and all chaotic components not linked to the largest one. These cells remain permanently empty for all N. There is an approximately Gaussian distribution around the mean value $\mu = \langle M \rangle = N/N_c$, where $N_c = \chi_A L^2$, with $L = 1000$, and thus approximately $\mu \approx 62.5$, for $L = 1000$, $N = 5 \times 10^7$, and $\chi_A \approx 0.80$. The numerical value of σ^2 is slightly larger, $\sigma^2 = 72$. In between we observe a shallow minimum, sparsely populated. Further work along these lines is in progress [36].

V. DISCUSSION AND CONCLUSIONS

In conclusion we may say that the major aspects of global diffusion in the stadium billiard are well understood, and that many aspects can be manifested in other systems with slow ergodicity. The applicability of the random model [35] is largely confirmed, the coarse grained phase space divided into cells is being filled exponentially. The diffusion constant obeys the parabolic law $D = D_0(\varepsilon)(1 - p^2)$, which we may expect to apply in other slow ergodic billiards as well. The distribution function emanating from an arbitrary initial condition obeys very well the inhomogeneous diffusion equation, and the diffusion is normal for all ε and initial conditions p_0. The boundary effects in the evolution of $\rho(p,t)$ are correctly

described by the model. The approach to uniform equilibrium distribution $\rho = 1/2$ with the variance $\text{Var}(p) = 1/3$ is always exponential, for all ε and all initial conditions p_0. The diffusion constant D_0 has been calculated for many different values of ε. At small $\varepsilon \leqslant \varepsilon_c \approx 0.1$ $D_0 \propto \varepsilon^{5/2}$, while for larger $\varepsilon \geqslant \varepsilon_c \approx 0.1$ it goes as $\propto \varepsilon^2$, in agreement with the previous works [4,22], but in between there is no theoretical analytical approximation, so we have to resort to the numerical calculations performed in this work. The value of the classical transport (diffusion) time N_T, in terms of the discrete time (number of collisions), has been determined for all values of $\varepsilon \leqslant 0.2$, which plays an important role in the quantum chaos of localized chaotic eigenstates [9,10,21].

In the mixed type systems, exemplified by the billiard introduced in the Ref. [27], with the shape parameter $\lambda = 0.15$, we have shown that the behavior is quite different from ergodic fully chaotic systems, which is in agreement with the report of Meiss [26] on the standard map.

Further work along these lines is important for the understanding of classical and quantum chaos in billiard systems as model systems, but the approach should also be applicable to other smooth Hamiltonian systems, such as, e.g., the hydrogen atom in a strong magnetic field [37–40], or the helium atom, etc.

[1] L. A. Bunimovich, Commun. Math. Phys. **65**, 295 (1979).

[2] M. V. Berry, Eur. J. Phys. **2**, 91 (1981).

[3] G. Benettin, Physica D **13**, 211 (1984).

[4] F. Borgonovi, G. Casati, and B. Li, Phys. Rev. Lett. **77**, 4744 (1996).

[5] H.-J. Stöckmann, *Quantum Chaos: An Introduction* (Cambridge University Press, Cambridge, England, 1999).

[6] F. Haake, *Quantum Signatures of Chaos* (Springer, Berlin, 2001).

[7] M. Robnik, Nonlinear Phenom. Complex Syst. (Minsk, Belarus) **1**, 1 (1998).

[8] B. Batistić and M. Robnik, J. Phys. A: Math. Theor. **43**, 215101 (2010).

[9] B. Batistić and M. Robnik, J. Phys. A: Math. Theor. **46**, 315102 (2013).

[10] B. Batistić and M. Robnik, Phys. Rev. E **88**, 052913 (2013).

[11] G. Casati, B. V. Chirikov, F. M. Izrailev, and J. Ford, Lect. Notes Phys. **93**, 334 (1979).

[12] B. V. Chirikov, F. M. Izrailev, and D. L. Shepelyansky, Sov. Sci. Rev. C **2**, 209 (1981).

[13] B. V. Chirikov, F. M. Izrailev, and D. L. Shepelyansky, Physica D **33**, 77 (1988).

[14] F. M. Izrailev, Phys. Rep. **196**, 299 (1990).

[15] F. M. Izrailev, Phys. Lett. A **134**, 13 (1988).

[16] F. M. Izrailev, J. Phys. A: Math. Gen. **22**, 865 (1989).

[17] B. Batistić, T. Manos, and M. Robnik, Europhys. Lett. **102**, 50008 (2013).

[18] T. Manos and M. Robnik, Phys. Rev. E **87**, 062905 (2013).

[19] T. Manos and M. Robnik, Phys. Rev. E **89**, 022905 (2014).

[20] T. Manos and M. Robnik, Phys. Rev. E **91**, 042904 (2015).

[21] B. Batistić, Č. Lozej, and M. Robnik (unpublished).

[22] G. Casati and T. Prosen, Physica D **131**, 293 (1999).

[23] T. Prosen, *in Proceedings of the International School in Physics "Enrico Fermi," Course CXLIII*, edited by G. Casati and U. Smilansky (IOS, Amsterdam, 2000).

[24] I. Dana, N. W. Murray, and I. C. Percival, Phys. Rev. Lett. **62**, 233 (1989).

[25] Q. Chen, I. Dana, J. D. Meiss, N. W. Murray, and I. C. Percival, Physica D **46**, 217 (1990).

[26] J. D. Meiss, Physica D **74**, 254 (1994).

[27] M. Robnik, J. Phys. A: Math. Gen. **16**, 3971 (1983).

[28] A. D. Polyanin, *Handbook of Linear Partial Differential Equations for Engineers and Scientists* (Chapman & Hall/CRC, Boca Raton, 2002).

[29] A. W. C. Lau and T. C. Lubensky, Phys. Rev. E **76**, 011123 (2007).

[30] L. A. Santaló and M. Kac, *Integral Geometry and Geometric Probability*, Cambridge Mathematical Library (Cambridge University Press, Cambridge, England, 2004).

[31] F. Vivaldi, G. Casati, and I. Guarneri, Phys. Rev. Lett. **51**, 727 (1983).

[32] D. N. Armstead, B. Hunt, and E. Ott, Physica D **193**, 96 (2004).

[33] E. G. Altmann, T. Friedrich, A. E. Motter, H. Kantz, and A. Richter, Phys. Rev. E **77**, 016205 (2008).

[34] R. Markarian, Nonlinearity **6**, 819 (1993).

[35] M. Robnik, J. Dobnikar, A. Rapisarda, T. Prosen, and M. Petkovšek, J. Phys. A: Math. Gen. **30**, L803 (1997).

[36] Č. Lozej and M. Robnik (unpublished).

[37] M. Robnik, J. Phys. A: Math. Gen. **14**, 3195 (1981).

[38] M. Robnik, J. Phys., Colloq. **43**, C2-45 (1982).

[39] H. Hasegawa, M. Robnik, and G. Wunner, Prog. Theor. Phys. Suppl. (Kyoto) **98**, 198 (1989).

[40] H. Friedrich and H. Wintgen, Phys. Rep. **183**, 37 (1989).

[41] Available at https://github.com/benokit/time-dep-billiards.